A suspended plate viscosity sensor featuring in-plane vibration and piezoresistive readout

C Riesch[1], E K Reichel[2], A Jachimowicz[1], J Schalko[1], P Hudek[3], B Jakoby[2], and F Keplinger[1]

[1] Institute of Sensor and Actuator Systems, Vienna University of Technology, Gusshausstrasse 27-29/366, 1040 Vienna, Austria

[2] Institute for Microelectronics and Microsensors, Johannes Kepler University, Altenberger Strasse 69, 4040 Linz, Austria

[3] Research Centre for Microtechnologies, Vorarlberg University of Applied Sciences, Hochschulstrasse 1, 6850 Dornbirn, Austria

E-mail: christian.riesch@alumni.tuwien.ac.at

Abstract. Miniaturized viscosity sensors are often characterized by high resonance frequencies and low vibration amplitudes. The viscosity parameter obtained by such devices is therefore not always comparable to those probed by conventional laboratory equipment. We present a novel micromachined viscosity sensor with relatively low operating frequencies in the kHz range. The sensor utilizes Lorentz force excitation, and piezoresistive readout. The resonating part consists of a rectangular plate suspended by four beam springs. The first mode of vibration is an in-plane mode. Thus, the contribution of the moving plate to the device damping is low, whereas the overall mass is high. This principle improves the quality factor and gives additional freedom to the device designer. The article presents the device concept, the fabrication process, and a prototype of the viscosity sensor. Measurement results demonstrate the feasibility of the device and show that the damping of the device is an appropriate measure for the viscosity.

PACS numbers: 83.85.Jn, 85.85.+j

Submitted to: *J. Micromech. Microeng.*

1. Introduction

Online monitoring of liquids often requires the measurement of the viscosity. Typical examples of conventional laboratory equipment apply rotating cylinders or cones [1]. However, this equipment requires sophisticated mechanical parts resulting in high costs. The taking of samples is time-consuming and error-prone. These reasons hamper the introduction of viscosity measurement for online monitoring. Miniaturized sensors, however, are a promising alternative to conventional laboratory equipment. In current research, viscosity sensors like thickness shear mode (TSM) quartz resonators or surface acoustic wave (SAW) devices were successfully used [2, 3]. These devices are characterized by operation frequencies in the MHz range. It is therefore clear, that the viscosity parameter obtained by such sensors is not always comparable to the results of laboratory equipment measuring at steady state or low-frequency oscillatory motion [4].

In contrast, resonant viscosity sensors based on micromachined moving structures operate at lower frequencies. These sensors probe the low-frequency behaviour of liquids, that is comparable to the steady shear viscosity measured by laboratory viscometers. Thus, they are better suited for the measurement of complex-structured or non-Newtonian liquids. This was confirmed by recent measurements with U-shaped cantilevers probing engine oil [5] and clamped-clamped beams immersed in suspensions of SiO_2 nano-particles and water [4].

A variety of micromachined sensors for viscosity can be found in the literature. The evaluation of the frequency spectra of atomic force microscope (AFM) cantilevers allows the simultaneous measurement of viscosity and density [6, 7, 8]. Other designs are based on Lorentz force actuated cantilevers [9] and clamped-clamped beams [10]. We recently presented a sensor system based on a micromachined vibrating beam excited by Lorentz forces and featuring optical readout [11]. This beam vibrates in an out-of-plane mode, which is mandatory for an optical readout mechanism. The flow field around the beam is rather complex with a significant damping due to compressional waves [12]. This damping leads to small vibration amplitudes, and, therefore, requires sophisticated readout techniques and circuitry. In contrast, sensors exciting mainly shear waves, like the TSM resonator, feature much higher quality factors [13].

The novel suspended plate sensor aims at improving the quality factor of micromachined viscosity sensors. The basic concept of this device is a thin plate vibrating in the in-plane direction. The plate is suspended by thin silicon beam springs. If the plate is thin enough, mainly shear waves would be excited in the surrounding liquid. Consequently, the damping of the vibrating part would be kept low, and high Q-factors can be achieved [14]. The most critical step in the fabrication of the sensor is the dicing process. The device must withstand the impact of cooling water of the wafer saw while the plate and the spring beams are already released from the handle wafer. When submerging the sensor in the sample liquid or removing it from the liquid, forces are exerted on the vibrating part. For sufficient mechanical stability, the presented MEMS (microelectromechanical system) device features rather thick plates and beams. In fact,

the geometric parameters of the springs are comparable to those of the clamped-clamped beam in [11]. As a result, the damping of the entire device is again dominated by the damping of the beams with rectangular cross-section, and the increase of the quality factor is moderate. However, the results given below indicate, that higher Q-factors can be achieved by varying the device dimensions. Also, the devices have proven sufficiently stable. Therefore, the thickness of the moving part could be further decreased. Due to the displacement amplitude in the micrometer range, our sensor is intended for liquids with larger structural length scales, whereas the amplitude of high frequency sensors is far below.

The vibrating structure consists of p-doped silicon, which is intrinsically piezoresistive. This effect is utilized to read out the plate deflection. The applied design eliminates the need for additional fabrication steps to deposit piezoelectric or piezoresistive material, or additional doping processes [15, 16]. The sensor device including excitation and readout is fabricated with a three-mask process. The output voltage of the Wheatstone bridge formed by the piezoresistive elements is in the range of only several µV. However, the excitation frequency is well known, and lock-in amplifiers and modulation techniques can be used to achieve a satisfying signal-to-noise ratio.

2. Sensor design

Figure 1 depicts the schematics of the novel sensor device. The main element is a rectangular plate suspended by four beam springs. The springs are 5 µm wide, and 20 µm high. Thus, their favoured direction of deflection is in the x–y plane, leading to in-plane vibrations of the suspended plate. The beams carry a conductive layer with the sinusoidal excitation current $i_\mathrm{e}(t)$. In the field of a permanent magnet (flux density $\vec{B} = -\vec{e}_z B_z$) Lorentz forces excite lateral vibrations of the plate and the springs. The ends of two beam springs (bottom of figure 1) are forked. Two of the prongs carry the excitation current whereas the other two form piezoresistive elements. Depending on the deflection of the vibrating plate, those piezoresistors are subject to either compressive or tensile stress. Their electric resistances change accordingly. With two additional constant resistors, they form a Wheatstone bridge circuit. The sensor readout is driven by a voltage $u_\mathrm{r}(t)$, and yields a differential output voltage $u_\mathrm{d}(t)$.

2.1. Modelling

For the sensor design, we used a simple model for the interaction of the vibrating parts with the surrounding fluid. Whereas the device operation in vacuum can be easily determined by finite element tools, it is preferable to describe its behaviour in a fluid by analytical or semi-analytical models to reduce the required computing power.

The interaction of the four springs (figure 2) with the surrounding liquid was modelled by approximating the rectangular beam by a beam with circular cross-section [17, 18]. Thus, we obtain the added mass due to the liquid loading per unit length

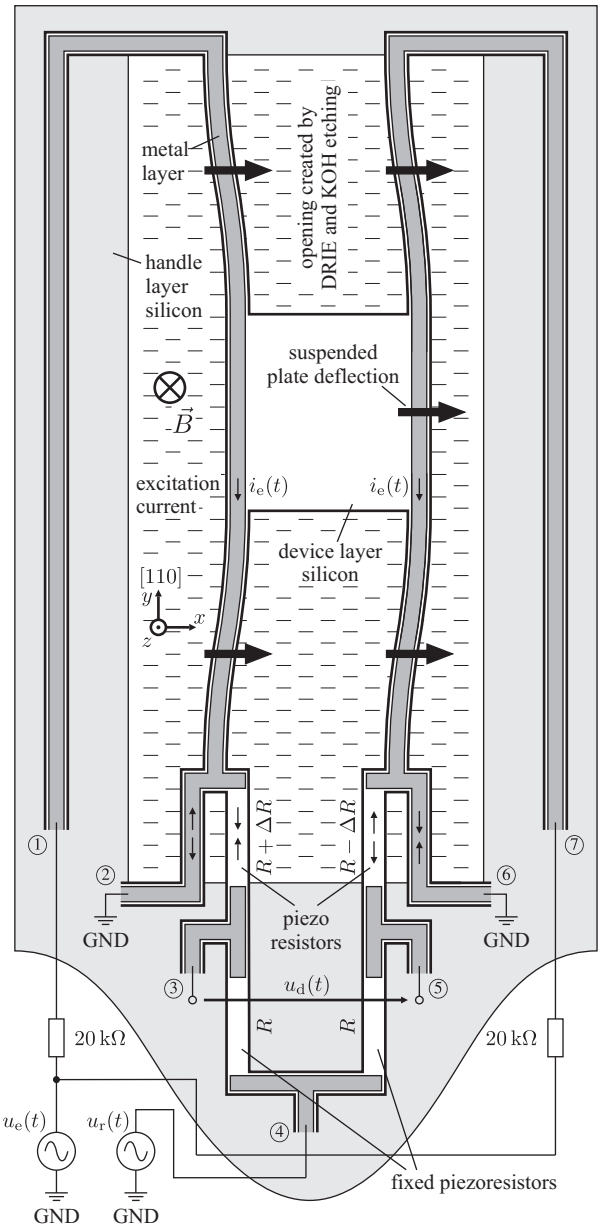

Figure 1. Schematic of the micromachined viscosity sensor. The in-plane movement of the plate is excited by the Lorentz forces arising from the excitation current $i_e(t)$ (sinusoidal, frequency f_e) and the magnetic flux density $\vec{B}$. The actual deflection is detected by a Wheatstone bridge of four piezoresistors (p-Si). Two of them are fixed, and two are mechanically stressed by the beam deflection. The Wheatstone bridge is fed with a sinusoidal voltage $u_r(t)$ at a frequency f_r. A lock-in amplifier locked to the difference frequency $f_r - f_e$ detects the beam deflection. This principle eliminates crosstalk from the excitation current and the baseline of the readout voltage.

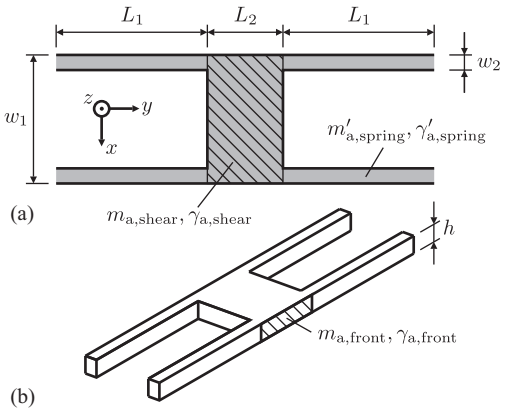

Figure 2. Model of the suspended plate device

$$m'_{\mathrm{a,spring}} = \rho\frac{\pi}{4}h^2\Gamma', \tag{1}$$

and the added damping coefficient per unit length

$$\gamma'_{\mathrm{a,spring}} = \rho\frac{\pi}{4}h^2\omega\Gamma'', \tag{2}$$

where ρ is the mass density of the liquid, and ω is the angular vibration frequency. $\Gamma = \Gamma' + \mathrm{j}\Gamma''$ is the hydrodynamic function

$$\Gamma = 1 + \frac{4\mathrm{j}K_1(-\mathrm{j}\sqrt{\mathrm{jRe}})}{\sqrt{\mathrm{jRe}}K_0(-\mathrm{j}\sqrt{\mathrm{jRe}})}, \tag{3}$$

where $\mathrm{Re} = \rho\omega h^2/(4\eta)$, and K_0 and K_1 are modified Bessel functions of the second kind [17]. η is the dynamic viscosity of the liquid.

The in-plane movement of the rectangular plate (hatched area in figure 2(a)) is expected to excite mainly shear waves in the liquid. Therefore, a one-dimensional model was employed that is commonly used for thickness shear mode resonators [19]. The mechanical stress acting on a plane at $z = 0$ that is oscillating harmonically in x-direction, and is in contact with a liquid, is given by [20]

$$\sigma_{zx} = \sqrt{\frac{\omega\eta\rho}{2}}(\mathrm{j} - 1)v_x, \tag{4}$$

where v_x is the velocity of the plate, $v_x = \hat{v}_x \exp(-\mathrm{j}\omega t)$. Therefore, the force acting on a vibrating rectangular plate (figure 2) which is in contact with the liquid on both sides is approximated by

$$F_x = 2w_1L_2\sigma_{zx} = -2w_1L_2\sqrt{\frac{\omega\eta\rho}{2}}v_x + 2w_1L_2\sqrt{\frac{\eta\rho}{2\omega}}\mathrm{j}\omega v_x. \tag{5}$$

This force F_x represents an additional mass loading of the sensor element,

$$m_{\mathrm{a,shear}} = 2w_1L_2\sqrt{\frac{\eta\rho}{2\omega}}, \tag{6}$$

and an additional damping

$$\gamma_{\mathrm{a,shear}} = 2w_1L_2\sqrt{\frac{\omega\eta\rho}{2}}. \tag{7}$$

Clearly, the front faces of the rectangular plate (hatched area in figure 2(b)) with respect to the direction of motion must be considered, too. In our simplified model, we use equations (1) and (2) again and multiply by the length of the plate,

$$m_{\mathrm{a,front}} = m'_{\mathrm{a,spring}} L_2, \tag{8}$$

and

$$\gamma_{\mathrm{a,front}} = \gamma'_{\mathrm{a,spring}} L_2. \tag{9}$$

The quality factor Q of a resonator is given by

$$Q = 2\pi \frac{W_{\mathrm{kin}}}{W_{\mathrm{loss},T}}, \tag{10}$$

where W_{kin} represents the peak kinetic energy of the system, and $W_{\mathrm{loss},T}$ is the dissipated energy per cycle (per time period $T = 2\pi/\omega$) [21].

We approximate the two pairs of springs as clamped-clamped beams, vibrating at their first mode of vibration. The kinetic energy contribution of such a beam immersed in liquid is

$$\begin{aligned} W_{\mathrm{beam}} &= \frac{1}{2} \int_0^L m' \left[\omega \hat{\psi} \varphi(y)\right]^2 \mathrm{d}y = \\ &= \frac{1}{2} (\rho_{\mathrm{d}} w_2 h + m'_{\mathrm{a,spring}}) \omega^2 \hat{\psi}^2 \int_0^L \varphi^2(y) \mathrm{d}y, \end{aligned} \tag{11}$$

where $\hat{\psi}$ is the peak deflection of the resonator in x-direction, $L = 2L_1$ is the length of the beam, $\varphi(y)$ is the normalized mode shape of first mode of resonance of a clamped–clamped rectangular beam, and ρ_{d} is the mass density of the device. $\varphi(y)$ is calculated by applying the boundary conditions $\varphi(0) = 0$, $\mathrm{d}\varphi(0)/\mathrm{d}y = 0$, $\varphi(L) = 0$, $\mathrm{d}\varphi(L)/\mathrm{d}y = 0$, to the Euler-Bernoulli beam equation [22], yielding

$$\begin{aligned} \varphi(y) = {} & 0.6186 \sin\left(\frac{4.73}{L} y\right) - 0.6297 \cos\left(\frac{4.73}{L} y\right) \\ & - 0.6186 \sinh\left(\frac{4.73}{L} y\right) + 0.6297 \cosh\left(\frac{4.73}{L} y\right), \end{aligned} \tag{12}$$

and

$$\int_0^L \varphi^2(y) \mathrm{d}y = \alpha L, \tag{13}$$

with $\alpha = 0.39714$. It should be noted that $\varphi(y)$ represents only an approximation of the actual mode shape of the beam springs. The rectangular plate suspended by the springs acts as a concentrated force at $y = L/2$, and should therefore be considered by an improved model.

In a similar way, the peak kinetic energy in the plate suspended by the springs can be derived as

$$W_{\mathrm{plate}} = \frac{1}{2} \left(L_2 w_1 h \rho_{\mathrm{d}} + m_{\mathrm{a,shear}} + m_{\mathrm{a,front}}\right) \omega^2 \hat{\psi}^2. \tag{14}$$

The total kinetic energy is thus

$$W_{\mathrm{kin}} = 2W_{\mathrm{beam}} + W_{\mathrm{plate}}. \tag{15}$$

Again, the two pairs of springs are considered as two rectangular clamped–clamped beams. The averaged dissipated power per unit length due to the liquid surrounding such a beam is

$$P' = \frac{1}{2}\gamma'_{\mathrm{a,spring}}\omega^2\hat{\psi}^2\varphi(y), \tag{16}$$

where $\gamma'_{\mathrm{a,spring}}$ is the damping coefficient according to (2). Integrating equation (16) over the time period T and the length of the beam yields

$$W_{\mathrm{loss,beam}} = \int_0^L \int_0^T P' \mathrm{d}t\mathrm{d}y = 2\pi\omega\hat{\psi}^2\gamma'_{\mathrm{a,spring}}\alpha L. \tag{17}$$

Accordingly, the dissipated energy of the vibrating plate is

$$W_{\mathrm{loss,plate}} = \pi\omega\hat{\psi}^2(\gamma_{\mathrm{a,shear}} + \gamma_{\mathrm{a,front}}). \tag{18}$$

The total energy loss per cycle is thus

$$W_{\mathrm{loss},T} = 2W_{\mathrm{loss,beam}} + W_{\mathrm{loss,plate}}. \tag{19}$$

The resonator device itself is considered free of intrinsic losses, which is justified by the high quality factor of the MEMS device vibrating in air.

Equation (10), therefore, results in

$$Q = \omega\frac{2(\rho_{\mathrm{d}}w_2h + m'_{\mathrm{a,spring}})\alpha L + \rho_{\mathrm{d}}L_2w_1h + m_{\mathrm{a,shear}} + m_{\mathrm{a,front}}}{2\gamma'_{\mathrm{a,spring}}\alpha L + \gamma_{\mathrm{a,shear}} + \gamma_{\mathrm{a,front}}}. \tag{20}$$

At resonance frequency, the peak kinematic energy of the resonator, W_{kin}, equals the peak strain energy of the spring beams [21]. This strain energy associated with the bending of the beams is

$$W_{\mathrm{strain}} = EI\hat{\psi}^2\int_0^L\left[\frac{\mathrm{d}^2\varphi(y)}{\mathrm{d}y^2}\right]^2\mathrm{d}y = \frac{EI\hat{\psi}^2\beta}{L^3}, \tag{21}$$

where E and $I = tw_2^3/12$ are the Young's modulus and the area moment of inertia, respectively [22], and the mode-shape factor $\beta = 198.782$. From $W_{\mathrm{kin}}(\omega_0) = W_{\mathrm{strain}}$, equations (15), and (21), the angular resonance frequency of the first mode of the suspended plate device is derived as

$$\omega_0^2 = \frac{2EI\beta}{L^3\left[2(\rho_{\mathrm{d}}w_2h + m'_{\mathrm{a,spring}})\alpha L + \rho_{\mathrm{d}}L_2w_1h + m_{\mathrm{a,shear}} + m_{\mathrm{a,front}}\right]}. \tag{22}$$

It should be noted, that the additional masses due to the liquid loading depend on the angular frequency. Therefore, equation (22) represents an implicit equation for ω_0.

2.2. Modelling results

Based on the derived model, a variety of suspended plate sensors with different dimensions have been designed and fabricated. Table 1 summarizes the geometrical and mechanical parameters of the sensor that was used in the experiments. Using equations (20), and (22), we can estimate the quality factor and the resonance frequency of the sensor. In air (viscosity $\eta = 1.8{\cdot}10^{-5}$ Pa·s, density $\rho = 1.2\,\mathrm{kg/m^3}$), the calculated first

Parameter	Value
w_1	100 µm
w_2	5 µm
L_1	600 µm
L_2	100 µm
h	20 µm
ρ_d	2330 kg/m^3
E	169 GPa

Table 1. Geometrical and mechanical parameters of the sensor device (figure 2). The neutral axes of the beam springs coincide with the [1 1 0] crystal direction of the device. In this direction, the Young's modulus of silicon is 169 GPa [23].

Liquid	η [mPa · s]	ρ [kg/m^3]
ethanol	1.06	789
1-propanol	1.90	804
1-butanol	2.52	810
1-pentanol	3.44	814
1-hexanol	4.49	814
1-heptanol	5.94	822
1-octanol	7.37	827
1-nonanol	9.10	827
1-decanol	10.97	830

Table 2. Dynamic viscosity (at 25 °C) and mass density of the sample liquids used for model calculations and experiments [24, 1].

mode resonance frequency is 17.2 kHz, and the quality factor is 292. As sample liquids, a variety of alcohols were used in the measurements. Table 2 lists their dynamic viscosities and mass densities. Immersed in these liquids, the plate resonator's resonance frequency f_0 will be in the range of 12.7 kHz to 9.4 kHz, according to the model, and the quality factor Q will drop to 3.1 for ethanol and 1 for decanol (table 3). The calculated resonance frequencies are thus in a similar range as those of the clamped-clamped beam sensor presented in [4]. The quality factors predicted by the models are fairly low, but we will show, that the achieved deflection amplitudes are still high enough for good readout sensitivity.

Another interesting modelling result is given by the added masses and damping coefficients due to the liquid loading. Table 3 lists the contributions of the beam springs ($m_\mathrm{a,spring}$, $\gamma_\mathrm{a,spring}$), the rectangular plate ($m_\mathrm{a,shear}$, $\gamma_\mathrm{a,shear}$), and the plate front face ($m_\mathrm{a,front}$, $\gamma_\mathrm{a,front}$) as defined in section 2.1. The results indicate, that the influence of the beam springs on the overall damping is much higher than that of the suspended plate itself. Increasing the width of the suspended plate w_1, would therefore have a low impact on the power loss per vibration cycle. However, the associated increase of

Liquid	f_0 [kHz]	Q	$m_{\mathrm{a,spring}}$ [ng]	$m_{\mathrm{a,shear}}$ [ng]	$m_{\mathrm{a,front}}$ [ng]	$\gamma_{\mathrm{a,spring}}$ [10^{-6}kg/s]	$\gamma_{\mathrm{a,shear}}$ [10^{-6}kg/s]	$\gamma_{\mathrm{a,front}}$ [10^{-6}kg/s]
ethanol	12.66	3.14	514	22.9	53.9	27.7	1.82	2.91
1-propanol	12.06	2.34	629	31.7	66.0	39.2	2.40	4.11
1-butanol	11.68	2.04	701	37.3	73.6	46.5	2.74	4.88
1-pentanol	11.30	1.75	794	44.4	83.3	56.1	3.15	5.89
1-hexanol	10.92	1.54	888	51.6	93.1	66.0	3.54	6.92
1-heptanol	10.46	1.35	1015	60.9	106	78.8	4.01	8.26
1-octanol	10.12	1.22	1128	69.2	118	90.4	4.40	9.48
1-nonanol	9.78	1.11	1253	78.3	132	103	4.81	10.9
1-decanol	9.44	1.02	1386	87.6	145	117	5.20	12.2

Table 3. Added mass and damping coefficients at resonance frequency for the suspended plate resonator according to table 1 and the liquid parameters of table 2. For comparison, the mass and the damping coefficient of the spring are given as $m_{\mathrm{a,spring}} = 2m'_{\mathrm{a,spring}}\alpha L$ and $\gamma_{\mathrm{a,spring}} = 2\gamma'_{\mathrm{a,spring}}\alpha L$, see also equation (20).

the moving mass would clearly yield a higher quality factor, see equation (20). Given the same geometry of the beam springs, and therefore the same spring constant, the resonance frequency is decreased, making the sensor feasible for non-Newtonian liquids. As an example, we used the model equations to design a different sensor geometry. We considered shorter beam springs (L_1 = 350µm) and a larger rectangular plate (L_2 = 150 µm, w_1 = 500 µm). The mass of this plate was 3.5 µg. Surrounded by the same set of sample liquids (table 2), the new sensor exhibits resonance frequencies in the range from 15.78 kHz to 14.34 kHz, and strongly increased quality factors in the range from 10.9 to 3.1.

2.3. Lorentz force excitation

For the excitation of MEMS-based viscosity sensors, the use of Lorentz forces has some advantages over other actuating principles. Piezoelectric drives require additional deposition processes to create the actuators, and sometimes also subsequent polarisation steps. Electrostatic excitation would eliminate the need for such materials, but the common finger structures are accompanied by squeeze film damping, which decrease the quality factor. Lorentz force excitation is easily accomplished, as only a conductive layer is required on the device to carry the excitation current. However, an external permanent magnet is needed to provide the magnetic field. With modern materials, flux densities of 200 mT and above are easily achieved. These flux densities allow to keep the excitation current small. From experiences with the clamped-clamped beam device of [11], we have estimated a maximum excitation current in the range of several mA.

To calculate the deflection amplitudes of the suspended plate a simple finite element (FEM) simulation was done. The geometry of the device (see table 1 and figure 1) was modelled in Comsol Multiphysics. In the *2D Conductive Media DC* application mode,

the current distribution was simulated. The resulting current density $\vec{J} = (J_x, J_y)$ was then used to calculate the force per unit area acting on the resonator, $\vec{J} \times \vec{B}$. The mechanical deflection was obtained from using Comsol Multiphysics' *Plain Strain* application mode and the material parameters of single-crystal silicon. A dc excitation current of 1 mA on each spring was applied and a magnetic flux density of $B_z = 200\,\mathrm{mT}$ was assumed. The simulation resulted in a static plate deflection of 36 nm.

2.4. Piezoresistive readout

Up to now, the sensor element was described as a rectangular plate suspended by four beams in the centre of an opening in the silicon device (figure 2). This vibrating part is actuated by Lorentz forces arising from a permanent magnetic field and the sinusoidal electric currents that are driven through conductive layers on the beam structures. For the measurement of the resonance behaviour of the device, it is crucial to obtain the actual plate deflection. Therefore, two of the beam springs are forked at their ends (figure 1). When the suspended plate is deflected, one of the prongs is compressed while the other is strained. Furthermore, one of the prongs carries a conductive layer and serves as ground connection for the excitation current, whereas the second one is not metallized, but is provided with electrical contacts to form a piezoresistive element [16].

For the first mode of vibration, characterized by a plate deflection in x-direction (figure 1), the mechanical stress in the piezoresistors is mainly oriented in the y-direction, which coincides with the [1 1 0] crystal direction of the silicon wafer. In this direction, the longitudinal piezoresistive coefficient of p-doped silicon is

$$\pi_\mathrm{l} = \frac{1}{2}\left(\pi_{11} + \pi_{12} + \pi_{44}\right) = 7.18 \cdot 10^{-10}\,\mathrm{Pa}^{-1} \tag{23}$$

at ambient temperature [25, 16]. The change of resistance ΔR of the piezoresistive element is thus given by

$$\Delta R = \sigma_\mathrm{l} \pi_\mathrm{l} R_0, \tag{24}$$

where R_0 is the initial resistance of the element, and σ_l is the mean mechanical stress acting in the [1 1 0] direction.

Four piezoresistors form a Wheatstone bridge circuit driven by the readout voltage u_r. Assuming that their resistances are equal, the resulting output voltage is

$$u_\mathrm{d}(t) = \frac{1}{2} u_\mathrm{r} \frac{\Delta R(t)}{R_0} = \frac{1}{2} u_\mathrm{r} \pi_\mathrm{l} \sigma_\mathrm{l}(t). \tag{25}$$

Driving the Wheatstone bridge with a dc voltage u_r, exciting the resonator vibrations at a frequency f_e, and assuming linear operation of the sensor results in an output voltage

$$u_\mathrm{d} = A \cos(2\pi f_\mathrm{e} + \phi), \tag{26}$$

which is proportional to the plate deflection. Here, ϕ represents the phase shift between excitation current and plate deflection. Since the excitation frequency is well-known, a lock-in amplifier can be used to separate the voltage amplitude of interest from a possible dc offset that stems from inequalities of the piezoresistors. However, the sensor

readout will be disturbed by interference from the excitation current. Like in most electric systems, such interference can be caused by inductive or capacitive coupling. For the device layout given in figure 1, another possible source of crosstalk must be considered: Both the excitation loop and the Wheatstone bridge use a common ground connection (figure 1) with a resistance of approximately 3–4 Ω. In this ground connection the excitation current causes a voltage drop of several mV. Since the piezoresistors are not perfectly equal, this voltage drop will not be cancelled out completely in the Wheatstone bridge, and will therefore interfere with the sensor readout.

It is, therefore, beneficial to drive the piezoresistors with a sinusoidal voltage at the readout frequency f_r, $u_\mathrm{r} = \hat{u}_\mathrm{r}\cos(2\pi f_\mathrm{r} t)$. Then the output voltage of the Wheatstone bridge is

$$\begin{aligned} u_\mathrm{d} &= \frac{1}{2}\pi_\mathrm{l} u_\mathrm{r}(t)\sigma_\mathrm{l}(t) = \frac{1}{2}\pi_\mathrm{l}\hat{u}_\mathrm{r}\cos(2\pi f_\mathrm{r} t)\hat{\sigma}_\mathrm{l}\cos(2\pi f_\mathrm{e} t + \phi) = \\ &= \frac{1}{4}\pi_\mathrm{l}\hat{u}_\mathrm{r}\hat{\sigma}_\mathrm{l}\left\{\cos\left[2\pi(f_\mathrm{r} - f_\mathrm{e})t - \phi\right] + \cos\left[2\pi(f_\mathrm{r} + f_\mathrm{e})t + \phi\right]\right\}. \end{aligned} \tag{27}$$

Now, the plate deflection can be obtained from setting a lock-in amplifier to either $|f_\mathrm{r} - f_\mathrm{e}|$ or $|f_\mathrm{r} + f_\mathrm{e}|$, and the crosstalk from the excitation current to the sensor output is eliminated.

The dimensions of the piezoresistors are $50\times3\times20\,\mu\mathrm{m}^3$. The device layer of the SOI wafer, from which the piezoresistors are fabricated, is p-doped silicon with a dopant concentration of approximately $10^{17}\,\mathrm{cm}^{-3}$. This dopant concentration yields an optimum piezoresistive coefficient [25], and also allows the formation of ohmic contacts to the metal layer. The resistivity ρ_el of the device layer is in the range from 0.11 Ωcm to 0.21 Ωcm. Calculating the resistance yields

$$R_\mathrm{calc} = \frac{\rho_\mathrm{el}\,50\,\mu\mathrm{m}}{3\cdot 20\,\mu\mathrm{m}^2} = 917\ldots1750\,\Omega. \tag{28}$$

Since the quality factor of the resonance in liquid is expected to be very low, i.e., from 2 to 10, it is crucial for the piezoresistive readout to be sensitive enough to detect static deflections. The finite element simulation of section 2.3 results in a mean mechanic stress in the piezoresistors of $\sigma_\mathrm{l} = 74\,\mathrm{kPa}$. Using a readout voltage amplitude $\hat{u}_\mathrm{r}$ of 1 V, the resulting output voltage detected at the differential frequency $|f_\mathrm{e} - f_\mathrm{r}|$ is

$$\hat{u}_{\mathrm{d},|f_\mathrm{e}-f_\mathrm{r}|} = \frac{1}{4}\pi_\mathrm{l}\hat{u}_\mathrm{r}\hat{\sigma}_\mathrm{l} = 13.3\,\mu\mathrm{V}. \tag{29}$$

3. Fabrication

The sensor was fabricated on a 4-inch (1 0 0) silicon-on-insulator (SOI) wafer. The thickness of the device layer, the buried oxide layer, and the handle layer were 20 µm, 2 µm, and 350 µm, respectively. Both sides of the wafer were coated with a stack of silicon nitride and silicon oxide (figure 3(a)). The device silicon layer was p-doped featuring a resistivity in the range from 0.11 Ωcm to 0.21 Ωcm. First, the top side coating was removed by reactive ion etching (RIE, figure 3(b)). A 500 nm aluminium layer was vapor deposited and patterned using lift-off technique (figure 3(c)) to form the

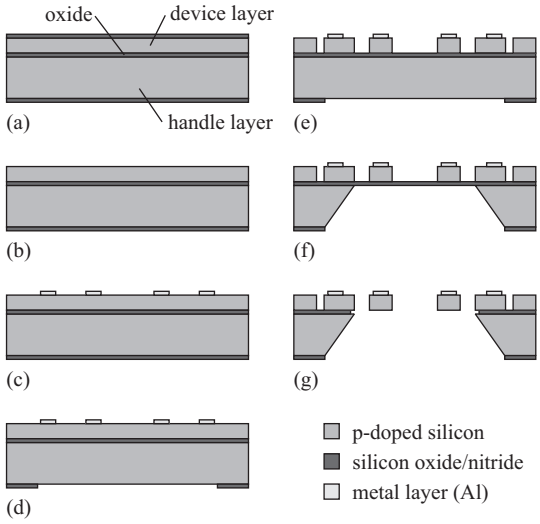

Figure 3. Simplified schematic of the fabrication process.

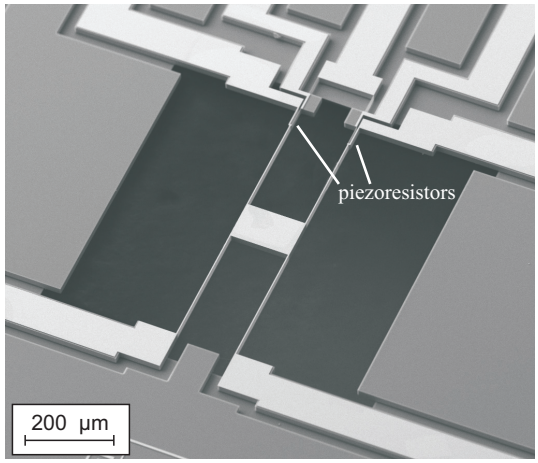

Figure 4. Scanning electron microscope (SEM) image of the suspended plate viscosity sensor. A magnified image of one of the piezoresistors is depicted in figure 5.

electrical connections. Subsequent annealing in vacuum was required to establish ohmic contacts between the metal layer and the silicon. Then openings were etched using RIE into the back-side nitride-oxide stack, which were required as mask for the KOH etching process (figure 3(d)). The free-standing structure, the piezo resistors, and the conducting paths were formed by deep reactive ion etching (pulsed-mode DRIE process using ICP plasma source — the inhibitor was added in time-multiplexed manner) on the wafer's front side (figure 3(e)). Subsequently, the wafer was KOH etched from the back-side (figure 3(f)), and the plate and the suspension springs were released by wet etching with buffered hydrofluoric acid (figure 3(g)). Figures 4 and 5 are scanning electron microscope (SEM) images of the sensor device and of one of the piezoresistive elements. After wafer dicing, the sensor devices were die-bonded on small printed circuit boards (PCB), and the electrical connections from chip to PCB were established by gold

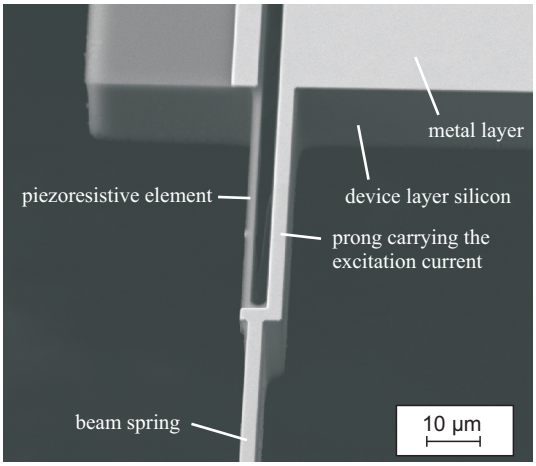

Figure 5. SEM image of the forked end of a beam spring, featuring a conductive layer for carrying the excitation current, and a piezoresistive element.

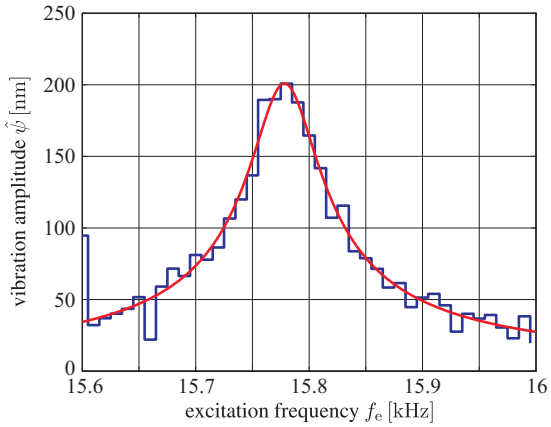

Figure 6. Frequency sweep measurement of the vibration amplitude of the sensor vibrating in air (excitation current amplitude $\hat{i}_e = 10\,\mu A$, flux density $B_z = 320\,mT$), obtained from the planar motion analyser of a Polytec MSA-400 microsystem analyser. The stair plot depicts the measurement results, whereas the solid line represents a second order system fit. The resonance frequency of the sensor vibrating in air is 15.77 kHz, the quality factor Q is 256.

wire-bonding. Finally, the wire bonds were protected by an epoxy compound.

4. Experimental

First, the operation of the sensor in air was investigated. As the structure vibrates in an in-plane mode, the stroboscopic planar motion mode of a Polytec MSA-400 microsystem analyser was used. The result of a frequency sweep measurement is depicted in figure 6. The sensor was excited with a current amplitude of 10 µA supplied by the MSA-400, and the magnetic flux density of 320 mT of a permanent magnet. The resulting vibration amplitude is rather low and the optical measurement is highly influenced by thermal drift and noise, but we found that higher mechanical deflections lead to nonlinear spring

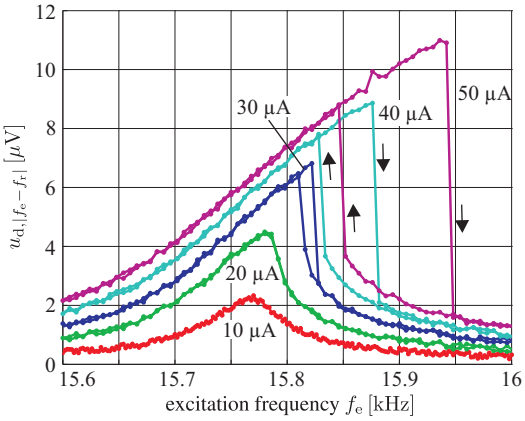

Figure 7. Frequency sweep experiments demonstrating the nonlinear Duffing behaviour of the resonator operating in air. Depending on the sweep direction indicated by the arrows the sensor exhibits a different frequency characteristic [26] at higher excitation currents. $u_{d,|f_e-f_r|}$ is the output voltage of the sensor's piezoresistive readout. The sensor was driven by a magnetic flux density of 320 mT and the excitation current amplitude stated in the figure. The results recorded for 10 µA correspond to the optical measurements of figure 6.

effects like the Duffing behaviour (figure 7). Nevertheless, the results give an idea of the sensor's resonance frequency $f_0 = \omega_0/(2\pi)$, quality factor Q, and maximum vibration amplitude $\hat{\psi}(\omega_0) = A_0 Q$. These parameters have been extracted by fitting the amplitude of a second order system,

$$\hat{\psi}(\omega) = \left| \frac{A_0}{1 + \mathrm{j}\omega \frac{1}{Q\omega_0} - \frac{\omega^2}{\omega_0^2}} \right|, \tag{30}$$

to the results. The fit is represented by the solid line in figure 6, and results in $f_0 = 15.77\,\mathrm{kHz}$, $Q = 256$, and $\hat{\psi}(\omega_0) = 200\,\mathrm{nm}$. The static beam deflection for excitation with 10 µA dc is obtained from $A_0 = 0.78\,\mathrm{nm}$. In addition, we used the scanning laser vibrometer of the microsystem analyzer to investigate the plate movements in the out-of-plane direction. No vibrations could be detected in the vicinity of the sensor's first-mode resonance frequency. As the vertical resolution of the vibrometer is in the range of several tens of femtometers, this measurement confirms the assumption of pure in-plane vibrations.

To characterize the piezoresistive elements electrically, their voltage–current characteristics were measured. In the range from −4 to 4 V, the resistances behave fairly ohmic. However, the measured resistance of 8.1 kΩ did not fit the calculated values (see section 2.4). This result indicates the presence of high contact resistances between the aluminium metallization and the semiconductor. Such sheet resistances R_S increase the total resistance in equation (25): R_0 must be replaced by $R_0 + 2R_S$, whereas ΔR is still given by equation (24), $\Delta R = \sigma_1 \pi_1 R_0$. Thus, the additional sheet resistances decrease the sensitivity of the piezoresistive readout.

Figure 8 describes the measurement setup for the integrated piezoresistive readout. Two Agilent 33220A function generators provided the excitation voltage u_e and the

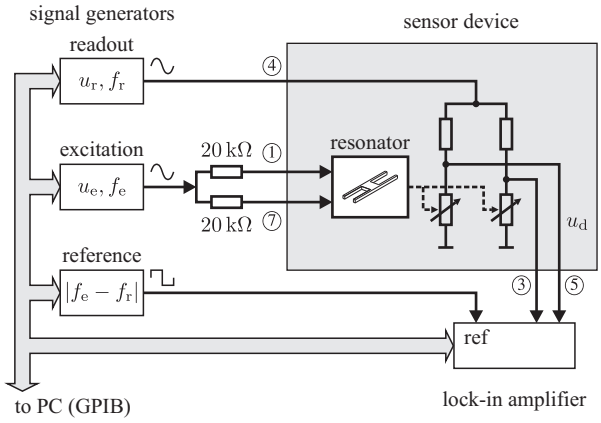

Figure 8. Schematic diagram of the measurement setup utilizing piezoresistive sensor readout. The circled numbers correspond to the sensor terminals in figure 1.

readout voltage u_r. In the excitation loops, 20 kΩ series resistors were placed (see also figure 1). The purpose of these resistors was to limit the excitation current. The maximum output voltage of the function generators was 10 V and, therefore, the excitation current was limited to 500 µA. A Stanford Research SR830 lock-in amplifier measured the differential voltage output of the sensor's bridge circuit. Due to the amplitude modulation in the piezoresistors (see section 2.4), the lock-in amplifier must be locked to either $f_r - f_e$ or $f_r + f_e$. A suitable reference signal for the lock-in amplifier can be generated by multiplying u_e with u_r. This multiplication results in a superposition of two sinusoidal signals at the frequencies $f_r - f_e$ and $f_r + f_e$. Subsequent filtering is required to suppress one of these signals. Due to the low excitation frequency f_e (down to 1 kHz) both the signals are very close in the frequency spectrum. A high order filter is required, which could potentially introduce an additional phase shift. To keep the setup simple in these first measurements a third function generator was used instead and set to $|f_e - f_r|$. The differential frequency was selected due to the limited frequency range of the lock-in amplifier. However, using a third signal source prohibits the measurement of the phase shift between excitation current and mechanical vibration, as the mutual phase shifts of the function generators are arbitrary.

In the first experiments, the excitation currents were kept low (amplitude of 500 µA), making sure not to destroy the device. To achieve reasonable vibration amplitudes and output voltages, we applied an electromagnet with a magnetic flux density of 1.9 T, instead. In later experiments, we determined a maximum excitation current of several mA, which allows reducing the magnetic flux density to a level that can easily be generated by a permanent magnet. In comparison to the microsystem analyser measurement, the excitation current was increased by a factor of 50, and the magnetic flux density by 5.9. An estimation of the static plate deflection in the following experiment is therefore $A_0 = 0.78\,\text{nm} \cdot 50 \cdot 5.9 = 230\,\text{nm}$.

The readout circuit was fed with a voltage of 1 V (amplitude) and a frequency of 99.4 kHz. The function generator that fed the excitation loop was set to an amplitude of

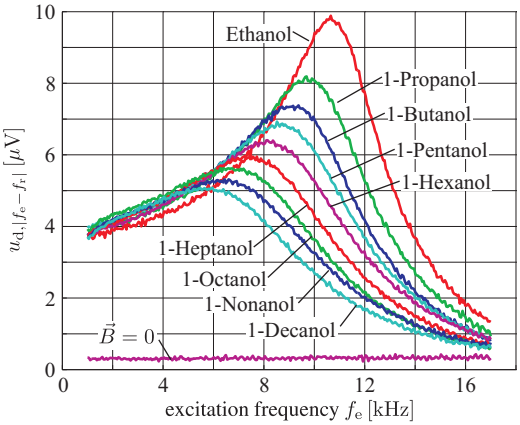

Figure 9. Resonance peaks of the suspended plate sensor immersed in a variety of nine sample liquids. The tenth result labeled $\vec{B} = 0$ was recorded with the electromagnet turned off, and indicates the noise floor.

10 V, resulting in an excitation current amplitude of 500 µA. The lock-in amplifier was configured for differential input, a sensitivity of 10 µV, and a time constant of 300 ms. A computer performed a frequency sweep measurement in the range from 2 to 17 kHz by changing the function generator frequencies f_e, and $|f_\mathrm{e} - f_\mathrm{r}|$, accordingly. The sensor was mounted in the centre of a $1{\times}1{\times}1\,\mathrm{cm}^3$ liquid container. This container was placed between the poles of the electromagnet and filled with 1 ml of liquid. The temperature of the liquids was 25 °C. A cover lid prevented evaporation of the fluids. As sample liquids, a variety of alcohols was chosen, which exhibit viscosities in the range from 1.06 to 10.97 mPa·s and densities from 789 to $830\,\mathrm{kg/m}^3$ (table 2). The sensor device was cleaned with ethanol between the measurements.

Figure 9 depicts the measurement results obtained with the nine sample liquids. To give an idea of the noise floor, a tenth curve was recorded with the sensor immersed in 1-decanol and with the electromagnet turned off. Again, the second order system, equation (30), was curve-fitted to the results of figure 9. Table 4 lists the resonance frequencies and the quality factors of the suspended plate sensor immersed in the liquids. The deviation of the modelling results (section 2.2) from the measurements are 15 % for the quality factor, and up to 30 % for the resonance frequency.

For the dynamic viscosity of the liquids and the damping factor $D = 1/(2Q)$, a simple relation was found, similar to that for the clamped–clamped beam [11, 10]. Figure 10 depicts both parameters in logarithmic scale.

5. Conclusions

To our knowledge, the presented device is the first micromachined viscosity sensor that is based on a plate vibrating in-plane. The feasibility of the novel viscosity sensor was demonstrated by experiments. The integrated piezoresistive readout is suitable to measure the frequency characteristics of the plate vibrations in liquids. The sensor

Liquid	f_0 [kHz]	D	Q
ethanol	10.71	0.18	2.75
1-propanol	9.92	0.23	2.17
1-butanol	9.38	0.26	1.92
1-pentanol	9.11	0.29	1.75
1-hexanol	8.82	0.30	1.64
1-heptanol	8.24	0.33	1.50
1-octanol	7.76	0.36	1.36
1-nonanol	7.64	0.39	1.27
1-decanol	7.18	0.42	1.20

Table 4. Results of curve-fitting a second order system, equation (30), to the measurement data of figure 9: f_0 is the resonance frequency, Q is the quality factor, and $D = 1/(2Q)$ is the damping factor.

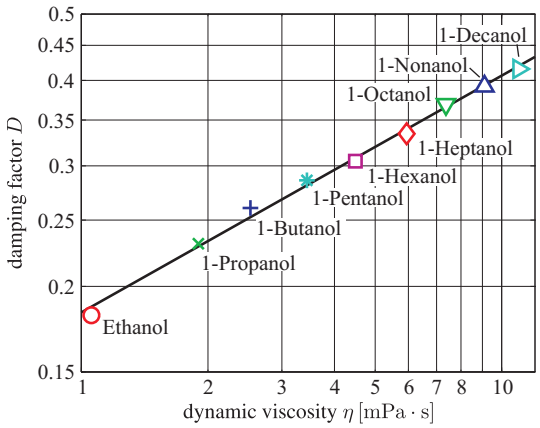

Figure 10. Damping factor D versus viscosity η. The markers indicate the measurement results, whereas the solid line depicts the fit result, $D = 1.998\eta^{0.346}$.

output voltages were in the range of up to 10 µV with a noise floor at 350 nV.

At the top and bottom faces of the rectangular plate, mainly shear waves are excited. Their contribution to the damping of the device is low. Therefore, increasing the size of the plate only results in a small increase of the damping, whereas the higher resonator mass enhances the quality factor. These increased Q-factors lead to higher deflection amplitudes, and better signal-to-noise ratios of the output voltage. We illustrated this relations with a model, resulting in Q-factors of up to 10.9 at a dynamic viscosity of 1.09 mPa·s. Such a Q-factor was already achieved by a clamped–clamped beam device presented in [10]. However, this resonating beam is characterized by a large thickness, increasing not only the moving mass, but also the stiffness of the device. Thus, the beam deflections were low, and required a highly sensitive readout, in particular a laser vibrometer.

Varying the size of the rectangular plate also allows the design of devices that exhibit different resonance frequencies. An array of such devices on a single chip would

probe the viscosity of liquids at several frequencies simultaneously, which could be a promising approach to measure the behaviour of viscoelastic fluids.

Acknowledgments

This work was supported by the Austrian Science Fund (FWF) Project L103-N07. The sensor device was fabricated at the Institute of Sensor and Actuator Systems, Vienna University of Technology (VUT), Austria, and the Research Centre for Microtechnologies, Vorarlberg University of Applied Sciences, Austria. The SEM image analysis was carried out using facilities at the University Service Centre for Transmission Electron Microscopy of the VUT.

References

[1] D. S. Viswanath, T. K. Ghosh, D. H. L. Prasad, N. V. K. Dutt, and K. Y. Rani, *Viscosity of Liquids*. Springer, 2007.

[2] E. Nwanko and C. J. Durning, "Fluid property investigation by impedance characterization of quartz crystal resonators (2 parts)," *Sens. Actuators A*, vol. 72, pp. 99–109 and 195–202, 1999. doi:10.1016/S0924-4247(98)00216-7

[3] B. Jakoby and M. J. Vellekoop, "Viscosity sensing using a Love-wave device," *Sens. Actuators A*, vol. 68, pp. 275–281, 1998. doi:10.1016/S0924-4247(98)00017-X

[4] C. Riesch, E. K. Reichel, A. Jachimowicz, F. Keplinger, and B. Jakoby, "A micromachined doubly-clamped beam rheometer for the measurement of viscosity and concentration of silicon-dioxide-in-water suspensions," in *IEEE Sensors Conf.*, Lecce, Italy, Oct. 26–29, 2008, pp. 391–394. doi:10.1109/ICSENS.2008.4716461

[5] A. Agoston, F. Keplinger, and B. Jakoby, "Evaluation of a vibrating micromachined cantilever for measuring the viscosity of complex organic liquids," *Sens. Actuators A*, vol. 123-124, pp. 82–86, 2005. doi:10.1016/j.sna.2005.02.020

[6] P. I. Oden, G. Y. Chen, R. A. Steele, R. J. Warmack, and T. Thundat, "Viscous drag measurements utilizing microfabricated cantilevers," *Appl. Phys. Lett.*, vol. 68, pp. 3814–3816, 1996. doi:10.1063/1.116626

[7] S. Boskovic, J. W. M. Chon, P. Mulvaney, and J. E. Sader, "Rheological measurements using microcantilevers," *J. Rheol.*, vol. 46, pp. 891–899, 2002. doi:10.1122/1.1475978

[8] N. McLoughlin, S. L. Lee, and G. Hähner, "Temperature dependence of viscosity and density of viscous liquids determined from thermal noise spectra of uncalibrated atomic force microscope cantilevers," *Lab Chip*, vol. 7, pp. 1057–1061, 2007. doi:10.1039/b705787c

[9] A. R. H. Goodwin, A. D. Fitt, K. A. Ronaldson, and W. A. Wakeham, "A vibrating plate fabricated by the methods of microelectromechanical systems (MEMS) for the simultaneous measurement of density and viscosity: Results for argon at temperatures between 323 and 423 K at pressures up to 68 MPa," *Int. J. Thermophys.*, vol. 27, pp. 1650–1676, 2006. doi:10.1007/s10765-006-0114-6

[10] I. Etchart, H. Chen, P. Dryden, J. Jundt, C. Harrison, K. Hsu, F. Marty, and B. Mercier, "MEMS sensors for density-viscosity sensing in a low-flow microfluidic environment," *Sens. Actuators A*, vol. 141, pp. 266–275, 2008. doi:10.1016/j.sna.2007.08.007

[11] C. Riesch, E. K. Reichel, A. Jachimowicz, F. Keplinger, and B. Jakoby, "A novel sensor system for liquid properties based on a micromachined beam and a low-cost optical readout," in *IEEE Sensors Conf.*, Atlanta, Georgia, USA, Oct. 28–31, 2007, pp. 872–875. doi:10.1109/ICSENS.2007.4388540

[12] B. Weiss, E. K. Reichel, and B. Jakoby, "Modeling of a clamped-clamped beam vibrating in a

fluid for viscosity and density sensing regarding compressibility," *Sens. Actuators A*, vol. 143, pp. 293–301, 2008. doi:10.1016/j.sna.2007.11.029

[13] S. J. Martin, V. Edwards Granstaff, and G. C. Frye, "Characterization of a quartz crystal microbalance with simultaneous mass and liquid loading," *Anal. Chem.*, vol. 63, pp. 2272–2281, 1991. doi:10.1021/ac00020a015

[14] J. H. Seo and O. Brand, "High Q-factor in-plane-mode resonant microsensor platform for gaseous/liquid environment," *J. Microelectromech. Syst.*, vol. 17, pp. 483–493, 2008. doi:10.1109/JMEMS.2008.916328

[15] J. Shajii, K.-Y. Ng, and M. A. Schmidt, "A microfabricated floating-element shear stress sensor using wafer-bonding technology," *J. Microelectromech. Syst.*, vol. 1, pp. 89–94, 1992. doi:10.1109/84.157363

[16] E. J. Eklund and A. M. Shkel, "Single-mask fabrication of high-G piezoresistive accelerometers with extended temperature range," *J. Micromech. Microeng.*, vol. 17, pp. 730–736, 2007. doi:10.1088/0960-1317/17/4/009

[17] J. E. Sader, "Frequency response of cantilever beams immersed in viscous fluids with applications to the atomic force microscope," *J. Appl. Phys.*, vol. 84, pp. 64–76, 1998. doi:10.1063/1.368002

[18] L. Rosenhead, Ed., *Laminar Boundary Layers*. Clarendon, 1963.

[19] K. K. Kanazawa and J. G. Gordon II, "The oscillation frequency of a quartz resonator in contact with a liquid," *Anal. Chim. Acta*, vol. 175, pp. 99–105, 1985. doi:10.1016/S0003-2670(00)82721-X

[20] L. D. Landau and E. M. Lifshitz, *Fluid Mechanics*. Pergamon Press, 1959.

[21] B. A. Auld, *Acoustic fields and waves in solids*. John Wiley & Sons, 1973, vol. 2.

[22] W. Weaver, Jr., S. P. Timoshenko, and D. H. Young, *Vibration problems in engineering*, 5th ed. John Wiley & Sons, 1990.

[23] J. J. Wortman and R. A. Evans, "Young's modulus, shear modulus, and poisson's ratio in silicon and germanium," *J. Appl. Phys.*, vol. 36, pp. 153–156, 1965. doi:10.1063/1.1713863

[24] D. R. Lide, Ed., *CRC Handbook of Chemistry and Physics*, 83rd ed. CRC Press, 2002.

[25] Y. Kanda, "Piezoresistance effect of silicon," *Sens. Actuators A*, vol. 28, pp. 83–91, 1991. doi:10.1016/0924-4247(91)85017-I

[26] B. Yurke, D. S. Greywall, A. N. Pargellis, and P. A. Busch, "Theory of amplifier-noise evasion in an oscillator employing a nonlinear resonator," *Phys. Rev. A*, vol. 51, pp. 4211–4229, 1995. doi:10.1103/PhysRevA.51.4211